Near-inertial parametric subharmonic instability of internal wave beams

Hussain H. Karimi and T. R. Akylas*
Department of Mechanical Engineering, Massachusetts Institute of Technology, Cambridge, Massachusetts 02139, USA
(Received 12 April 2017; published 14 July 2017)

Parametric subharmonic instability (PSI) of internal wave beams in a uniformly stratified fluid is discussed, for the case where the beam frequency is nearly twice the inertial frequency due to background rotation. Compared with generic PSI, beams of finite width are expected on physical grounds to be more vulnerable to subharmonic perturbations of near-inertial frequency, as these disturbances have small group velocity and stay in contact with the underlying beam longer, thus extracting more energy. A weakly nonlinear theory for such near-inertial PSI is developed in the "distinguished limit" where the effects of triad nonlinear interactions, dispersion, and viscous dissipation are equally important. This model is used to examine the linear stability of a uniform beam to infinitesimal perturbations under a "pump-wave" approximation, as well as the nonlinear development of PSI that takes into account the effect of the growing perturbations on the beam evolution. Near-inertial PSI is possible for beams of general locally confined profile, in sharp contrast to generic PSI which can arise only for quasimonochromatic beams whose profile comprises a sinusoidal carrier modulated by a locally confined envelope. The theoretical predictions are consistent with earlier numerical simulations of semidiurnal internal tide beams generated over the continental shelf break at latitudes above and below the critical value 28.8°N, at which the subharmonic semidiurnal frequency matches the local inertial frequency.

DOI: 10.1103/PhysRevFluids.2.074801

I. INTRODUCTION

The problem of parametric subharmonic instability (PSI) of a sinusoidal internal wave in a uniformly stratified fluid has received intensive study in the last 40 years. In this idealized setting, PSI is understood as a resonant triad wave interaction of the primary wave train with subharmonic perturbations that satisfy certain resonance conditions [1–3]. In the inviscid limit, in particular, the most unstable perturbations have frequency one half of the primary wave frequency and short wavelength; PSI thus provides a possible mechanism for transferring energy to smaller scales in a high Reynolds number environment and is believed to contribute to mixing in oceans (see Staquet and Sommeria [4] and references given therein).

By contrast, little attention has been paid to understanding PSI of internal waves under more realistic flow conditions [5]. In an attempt to fill this gap, recent theoretical [6,7], experimental [7–9], and numerical [9] work has focused on PSI of internal wave beams: time-harmonic plane waves with locally confined spatial profile. Such disturbances are characteristic manifestations of the anisotropy of internal wave motion [10] and can be readily generated by mechanical forcing in the laboratory [11,12]; furthermore, they arise naturally in oceans from the interaction of barotropic tidal flow with topography [13–15], as well as in the atmosphere due to thunderstorms [16]. Interestingly, unlike sinusoidal plane waves which invariably suffer PSI, wave beams do not always do so, and the beam profile turns out to be a major factor. Specifically, a systematic theoretical study (Karimi and Akylas [6]) of the weakly nonlinear interaction of a finite-width beam with subharmonic perturbations has pointed out that PSI is possible only if the beam profile is (i) quasimonochromatic so as to enable subharmonic perturbations to form finely tuned triads with the beam, and (ii) sufficiently wide (i.e., it

*trakylas@mit.edu

comprises a large enough number of carrier wavelengths, depending on the beam amplitude and the flow Reynolds number) for subharmonic perturbations, which propagate with their group velocities, to stay in contact with the beam long enough. The theoretical criteria for PSI of finite-width beams obtained in Ref. [6] are in keeping with numerical simulations [9] and laboratory experiments [7–9], even though the numerical and experimental flow conditions only marginally satisfied the assumptions of the weakly nonlinear theory [6,17].

This paper is a sequel to the asymptotic theory for PSI of internal wave beams developed in Karimi and Akylas [6]. An essential difference from our earlier work is that here we include Coriolis effects which become relevant in geophysical settings due to the Earth's rotation. Our primary goal, however, is to understand PSI in the particular, but all-important, case that the beam frequency is nearly twice the inertial frequency due to background rotation. Under this condition, beams of finite width are expected on physical grounds to be especially vulnerable to PSI, as subharmonic perturbations of near-inertial frequency have small group velocity and stay in contact with the underlying beam longer, thus extracting more energy, than subharmonic perturbations of general frequency. The prominent role of such near-inertial PSI is also brought out by numerical simulations [18] of semidiurnal tide beams generated over the continental shelf break. These beams feature profiles with no distinct carrier and thus would not experience PSI according to the theoretical criteria obtained in Ref. [6]. Yet, strong PSI is found at the particular latitude of 27.5°N, slightly below the critical value of 28.8°N where the semidiurnal frequency equals twice the local inertial frequency, whereas relatively minor or no instability is seen at 0°N and 45°N. In addition, there is numerical [19–21] as well as observational [22] evidence of significant energy transfer to near-inertial motions, via PSI, when internal tides cross this critical latitude.

The ensuing analysis provides theoretical confirmation of the decisive role of subharmonic perturbations with near-inertial frequency in causing PSI. Specifically, as suggested by the simulations of Gerkema *et al.* [18], it is shown that the small group velocity of such perturbations enables more robust resonant triad interactions with the underlying beam, enhancing instability in a dramatic way. Thus, beams with general locally confined profile are susceptible to near-inertial PSI, in sharp contrast to generic PSI which can arise only for beams with quasimonochromatic profile that comprise a large enough number of carrier wavelengths. However, this crucial distinction between near-inertial and generic PSI is no longer relevant if, instead of a finite-width beam, one considers a uniform sinusoidal wave train; resonant triad interactions in both types of PSI then involve monochromatic subharmonic perturbations so group velocity is not a factor.

Similar to the approach taken in Karimi and Akylas [6], we first derive a system of coupled evolution equations for the interaction of a small-amplitude wave beam with near-inertial subharmonic wave packets, in the "distinguished limit" where the effects of triad nonlinear interactions, dispersion, and viscous dissipation are equally important. This equation system is then used to examine the linear stability of a uniform beam, assuming its profile is "frozen," by solving an appropriate eigenvalue problem. Such a "pump-wave" approximation was also used by Young *et al.* [23] in discussing the near-inertial PSI of an internal tide, but their inviscid formulation did not provide a preferred wavelength of instability. By contrast, here we focus on a single beam including viscous dissipation, and our stability eigenvalue analysis yields a most unstable perturbation wavelength and associated growth rate; moreover, the coupled interaction equations derived here make it possible to trace the nonlinear development of PSI that takes into account the effect of the growing perturbations on the beam evolution. The theoretical predictions regarding the most unstable disturbance are in good qualitative, and reasonable quantitative, agreement with the PSI seen in the simulations of Gerkema *et al.* [18] at the near-critical latitude 27.5°N.

II. INTERACTION EQUATIONS

The present analysis assumes the same flow conditions as in Karimi and Akylas [6], namely, two-dimensional disturbances in an incompressible continuously stratified Boussinesq fluid of constant buoyancy frequency N_0, but with the addition of Coriolis effects due to the Earth's rotation. Also,

as before, we shall work with dimensionless variables, in terms of the time scale $1/N_0$ and a characteristic length scale L_* of the underlying wave beam. With x being the horizontal and y the vertical coordinate pointing upwards, the stream function $\psi(x,y,t)$ for the in-plane velocity field $(\psi_y,-\psi_x)$, the transverse velocity $w(x,y,t)$, and the reduced density $\rho(x,y,t)$ are then governed by

$$\rho_t + \psi_x + \mathrm{J}(\rho,\psi) = 0, \tag{1a}$$

$$w_t - f\psi_y + \mathrm{J}(w,\psi) - \nu\nabla^2 w = 0, \tag{1b}$$

$$\nabla^2\psi_t - \rho_x + f w_y + \mathrm{J}(\nabla^2\psi,\psi) - \nu\nabla^4\psi = 0, \tag{1c}$$

where $\mathrm{J}(a,b) = a_x b_y - a_y b_x$ is the Jacobian. The parameters

$$\nu = \frac{\nu_*}{N_0 L_*^2} \tag{2}$$

and

$$f = 2\frac{\Omega}{N_0}\sin\beta \tag{3}$$

are, respectively, the inverse Reynolds number and nondimensional inertial frequency, where ν_* denotes the kinematic viscosity, Ω the rotation rate of the Earth, and β the local latitude.

According to Eqs. (1), in the inviscid limit ($\nu = 0$), linear sinusoidal plane waves obey the dispersion relation

$$\omega^2 = f^2 + (1 - f^2)\sin^2\theta. \tag{4}$$

It should be noted that the wave frequency ω depends on the inclination θ to the vertical, but not the magnitude, of the wave vector. Thus, similar to the case of no background rotation ($f = 0$), it is possible to construct wave beams (i.e., time-harmonic plane waves with general profile) by superposing sinusoidal plane waves whose wave vectors have different magnitudes but all point in the same direction. The dispersion relation (4) then links the beam frequency $f < \omega < 1$ to the angle θ that the beam direction makes to the horizontal (see Fig. 1). Moreover, such infinitely long, uniform beams are exact nonlinear states of Eqs. (1) for $\nu = 0$, irrespective of the beam profile [10,24].

Focusing now on the stability of a uniform beam of frequency ω, PSI involves perturbations of short wavelength ($\lambda_*/L_* \ll 1$) and frequency close to $\omega/2$. According to Eq. (4), such perturbations have crests inclined to the horizontal by ϕ, where

$$\sin\phi = \sqrt{\frac{\omega^2/4 - f^2}{1 - f^2}}, \tag{5}$$

and the corresponding group velocity

$$\boldsymbol{c}_{g\pm} = \pm 2\frac{1 - f^2}{\omega k}\sin\phi\cos\phi(\cos\phi\hat{\boldsymbol{e}}_x - \sin\phi\hat{\boldsymbol{e}}_y) \tag{6}$$

is aligned with the wave crests, where k is the perturbation wave number modulus (see Fig. 1). We recall that, in the absence of background rotation, Karimi and Akylas [6] came to the conclusion that beams with locally confined profile do not experience PSI in general because subharmonic perturbations travel with their respective group velocity and triad interactions do not have enough time to act; PSI may arise only for sufficiently wide quasimonochromatic beams that comprise a large enough number of carrier wavelengths, depending on the beam amplitude and the Reynolds number $1/\nu$. In the present setting, by contrast, it is seen from Eqs. (5) and (6) that $\boldsymbol{c}_{g\pm} \to 0$ as $\omega/2 \to f$, suggesting that subharmonic perturbations with near-inertial frequency ($\omega/2 \approx f$) could extract energy more efficiently from a beam of finite width [18]. The ensuing analysis supports this claim, and near-inertial PSI is shown to be possible for beams with general localized profile.

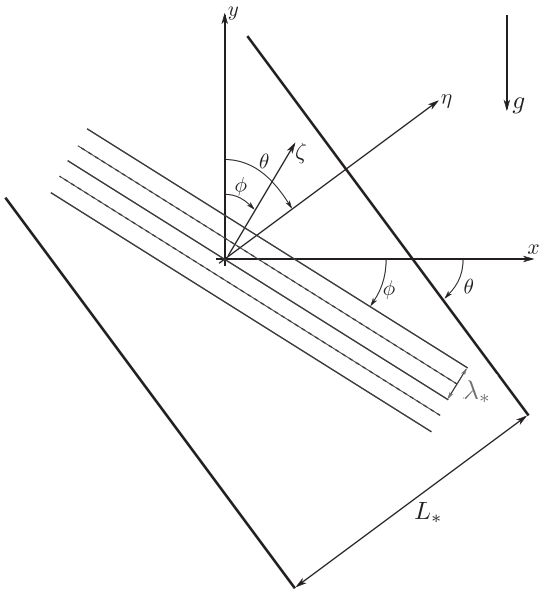

FIG. 1. Geometry of PSI. The underlying wave beam with general locally confined profile of characteristic width L_* has dimensionless frequency ω and propagates at angle θ to the horizontal in keeping with the dispersion relation (4). Subharmonic perturbations are short-crested ($\lambda_*/L_* \ll 1$) nearly monochromatic wave packets with dimensionless frequency close to $\omega/2$ that propagate at the angle ϕ to the horizontal determined by Eq. (5).

In preparation for the PSI analysis, we now derive evolution equations for the interaction of a wave beam with subharmonic perturbations of near-inertial frequency. As in Karimi and Akylas [6], we consider the "distinguished limit" where the effects of triad nonlinear interactions, dispersion, and viscous dissipation are assumed to be weak but equally important. The appropriate scalings turn out to be the same as those found in the absence of background rotation [6], save for the vanishing group velocity of near-inertial perturbations noted above.

Briefly, introducing the steepness parameter

$$\epsilon = \frac{U_*}{N_0 L_*} \ll 1, \tag{7}$$

where U_* is a (dimensional) characteristic beam velocity, we first require weakly nonlinear effects due to triad interactions to be comparable to the effects of dispersion due to the modulation of the short-scale perturbations by the underlying beam. From our earlier work [6], this balance is realized when the perturbation wave number $k = O(1/\epsilon^{1/2})$ so we write

$$k = \frac{\kappa}{\epsilon^{1/2}}, \tag{8}$$

where $\kappa = O(1)$ is a scaled wave number parameter; dispersive and nonlinear effects thus come into play on the same $O(1/\epsilon)$ time scale. Now, in order for triad interactions to have a chance to cause instability, this time scale must be also commensurate with the travel time of the perturbations, which propagate with the group velocity in Eq. (6), across the $O(1)$ beam width. Therefore, it is necessary that $\boldsymbol{c}_{g\pm} = O(\epsilon)$ and, according to Eqs. (5) and (8), this condition can be met only if the perturbations have near-inertial frequency ($\omega/2 \approx f$) so $\sin\phi = O(\epsilon^{1/2})$. Hence, we introduce the scaling

$$\sin\phi = \sigma\epsilon^{1/2}, \tag{9}$$

where $\sigma = O(1)$ is a parameter that according to Eq. (5) controls proximity of $\omega/2$ to the inertial frequency

$$\frac{\omega}{2} = f + \frac{\sigma^2(1-f^2)}{2f}\epsilon + \cdots . \tag{10}$$

Finally, in regard to viscous dissipation, the decay rate of internal waves is known to be proportional to νk^2 [25]. Thus, in view of Eq. (8), the scaling

$$\nu = \alpha\epsilon^2, \tag{11}$$

where $\alpha = O(1)$, brings viscous damping, which affects predominantly the short-scale perturbations, on par with nonlinearity and dispersion. Moreover,

$$T = \epsilon t \tag{12}$$

is the appropriate "slow" time variable for the evolution of the perturbations in the presence of these effects.

Taking into account the above scalings, we next expand the flow variables ψ, ρ, and w as follows:

$$\psi = \epsilon\{Q(\eta,T)e^{-i\omega t} + \text{c.c.}\} + \frac{\epsilon^{3/2}}{\kappa}\left\{\left[A(\eta,T)e^{i\kappa\zeta/\epsilon^{1/2}} + B(\eta,T)e^{-i\kappa\zeta/\epsilon^{1/2}}\right]e^{-i\omega t/2} + \text{c.c.}\right\} + \cdots , \tag{13a}$$

$$\rho = \epsilon\{R(\eta,T)e^{-i\omega t} + \text{c.c.}\} + \epsilon\left\{\left[F(\eta,T)e^{i\kappa\zeta/\epsilon^{1/2}} + G(\eta,T)e^{-i\kappa\zeta/\epsilon^{1/2}}\right]e^{-i\omega t/2} + \text{c.c.}\right\} + \cdots , \tag{13b}$$

$$w = \epsilon\{W(\eta,T)e^{-i\omega t} + \text{c.c.}\} + \epsilon\left\{\left[M(\eta,T)e^{i\kappa\zeta/\epsilon^{1/2}} + N(\eta,T)e^{-i\kappa\zeta/\epsilon^{1/2}}\right]e^{-i\omega t/2} + \text{c.c.}\right\} + \cdots . \tag{13c}$$

In the above expansions, the first curly brackets represent an $O(\epsilon)$ wave beam of frequency ω and propagation direction inclined at angle θ to the horizontal in keeping with the dispersion relation (4); the beam has general spatial profile described by the complex amplitudes Q, R, and W which vary in the across-beam direction $\eta = x\sin\theta + y\cos\theta$ (see Fig. 1). The second curly brackets stand for the subharmonic perturbation; it comprises two fine-scale wave packets with carrier wave vectors of the same magnitude $\kappa/\epsilon^{1/2}$ but opposite directions along $\zeta = x\sin\phi + y\cos\phi$, in keeping with Eqs. (5) and (8). These wave packets are modulated owing to their interaction with the underlying beam, so the envelopes A, B, F, G, M, and N are functions of η and the slow time T. Moreover, as a result of this long–short wave interaction, the perturbation may grow to be comparable to the $O(\epsilon)$ beam and affect the beam profile; to allow for such feedback, Q, R, and W are taken to be functions of T as well.

Upon substituting expansions (13) into the governing equations (1), we collect terms proportional to $\exp(-i\omega t)$ and $\exp(\pm i\kappa\zeta/\epsilon^{1/2})\exp(-i\omega t/2)$. The resulting nine coupled equations are then reduced, by consistent elimination of the rest of the unknowns, to three evolution equations for the beam profile amplitude Q and the wave packet envelopes A and B of the stream function in Eq. (13a). This rather heavy algebraic manipulation is simplified to some extent by making use of Eqs. (9) and (10) which hold for near-inertial subharmonic frequency (see the Appendix for details). Here, we quote the three evolution equations in final form:

$$Q_T + 2\gamma AB = 0, \tag{14}$$

$$A_T + \frac{\sigma c}{\kappa}A_\eta - \frac{i}{2}\frac{c'}{\kappa^2}A_{\eta\eta} + \alpha\kappa^2 A - i\delta\kappa^2 A|Q_\eta|^2 + \gamma Q_{\eta\eta}B^* = 0, \tag{15a}$$

$$B_T - \frac{\sigma c}{\kappa}B_\eta - \frac{i}{2}\frac{c'}{\kappa^2}B_{\eta\eta} + \alpha\kappa^2 B - i\delta\kappa^2 B|Q_\eta|^2 + \gamma Q_{\eta\eta}A^* = 0, \tag{15b}$$

where the coefficients

$$c = \sqrt{3(1-f^2)}, \quad c' = 3f, \quad \delta = \frac{3f}{2(1-f^2)}, \quad \gamma = \frac{3f\sqrt{3(1-4f^2)}}{4(1-f^2)} \tag{16}$$

depend only on the inertial frequency f and * denotes the complex conjugate. It should be noted that this system pertains to near-inertial PSI only ($\omega/2 \approx f$), and it is not possible from Eqs. (14) and (15) to recover the interaction equations obtained for $f = 0$ in Ref. [6].

The first two terms in Eqs. (15) represent the propagation of the subharmonic wave packet envelopes A and B across the beam with speed $\pm\epsilon\sigma c/\kappa = \boldsymbol{c}_{g\pm} \cdot \hat{\boldsymbol{e}}_\eta$, the projection of the respective group velocity [viz., Eq. (6)] on the across-beam direction η. The third and fourth terms account for the envelope dispersion and viscous dissipation, respectively. In addition, A and B are coupled to the beam amplitude Q via the nonlinear terms in Eqs. (14) and (15); these terms derive from triad interactions and allow energy exchange between the beam and subharhmonic perturbations. Owing to the scalings chosen earlier, all the above effects become equally important at $T = O(1)$. This balance is sensitive to the parameter σ, which controls the wave packet propagation speed. For subharmonic frequencies far from f, corresponding to $\sigma \gg 1$ according to Eq. (10), this speed becomes relatively large so perturbations have little time to interact with a locally confined beam, thus precluding PSI as concluded in Ref. [6].

The evolution equations (14) and (15) describe the full nonlinear coupling of a weakly nonlinear wave beam with fine-scale subharmonic wave packets of comparable amplitude. For the purposes of PSI analysis, however, subharmonic disturbances are taken to be relatively small, $|A|, |B| \ll |Q|$, and the nonlinear term in Eq. (14) can be neglected. Hence, in this so-called pump-wave approximation, the beam profile does not evolve with time, $Q(\eta, T) = \overline{Q}(\eta)$, and A, B are governed by

$$A_T + \frac{\sigma c}{\kappa} A_\eta - \frac{i}{2}\frac{c'}{\kappa^2} A_{\eta\eta} + \alpha\kappa^2 A - i\delta\kappa^2 A|\overline{Q}_\eta|^2 + \gamma\,\overline{Q}_{\eta\eta} B^* = 0, \tag{17a}$$

$$B_T - \frac{\sigma c}{\kappa} B_\eta - \frac{i}{2}\frac{c'}{\kappa^2} B_{\eta\eta} + \alpha\kappa^2 B - i\delta\kappa^2 B|\overline{Q}_\eta|^2 + \gamma\,\overline{Q}_{\eta\eta} A^* = 0. \tag{17b}$$

This linear system forms the basis of our analysis of near-inertial PSI below. We shall return to the full interaction equations (14) and (15) in Sec. IV C for discussing the long-time evolution of unstable disturbances.

III. SINUSOIDAL PLANE WAVE

We first examine the PSI of a uniform sinusoidal wave train

$$\overline{Q} = \tfrac{1}{2} e^{i\eta}. \tag{18}$$

Here, the wavelength is set to 2π (the characteristic length $L_* =$ dimensional wavelength$/2\pi$), and $\overline{Q}$ is normalized so that the peak amplitude of the beam stream function in Eq. (13a) is equal to ϵ.

Putting expression (18) into Eqs. (17), the linear stability problem centers on separable normal modes in the form

$$A = A_0 e^{\lambda T} e^{i\rho\eta}, \quad B = B_0 e^{\lambda^* T} e^{i(1-\rho)\eta}, \tag{19}$$

where the mode wave number ρ is real and $\lambda = \lambda_r + i\lambda_i$ is in general complex so instability arises if the growth rate $\lambda_r > 0$. In view of Eqs. (19), the subharmonic perturbations in Eq. (13a) have wave vectors

$$\boldsymbol{k}_+ = \frac{\kappa}{\epsilon^{1/2}}\hat{\boldsymbol{e}}_\zeta + \rho\hat{\boldsymbol{e}}_\eta, \quad \boldsymbol{k}_- = -\frac{\kappa}{\epsilon^{1/2}}\hat{\boldsymbol{e}}_\zeta + (1-\rho)\hat{\boldsymbol{e}}_\eta, \tag{20a}$$

and corresponding frequencies

$$\omega_+ = \frac{\omega}{2} - \lambda_i\epsilon, \quad \omega_- = \frac{\omega}{2} + \lambda_i\epsilon; \tag{20b}$$

hence,

$$\boldsymbol{k}_+ + \boldsymbol{k}_- = \hat{\boldsymbol{e}}_\eta, \quad \omega_+ + \omega_- = \omega, \tag{21}$$

so the modes defined by Eqs. (19) form (perfectly tuned) resonant triads with the underlying wave train of wave vector $\hat{\boldsymbol{e}}_\eta$ and frequency ω.

Upon substituting expressions (19) into Eqs. (17), the characteristic equation which determines the eigenvalue λ can be written in the form

$$\left\{(\lambda + \alpha\kappa^2) + \frac{i}{2}\left[\frac{\sigma c}{\kappa} - \frac{c'}{2\kappa^2}(1-2\rho)\right]\right\}^2 = \frac{1}{4}\gamma^2 - \frac{1}{2}\left\{\frac{2\sigma c}{\kappa}(2\rho-1) + \frac{c'}{\kappa^2}(2\rho^2 - 2\rho + 1) - \delta\kappa^2\right\}^2. \tag{22}$$

Now, varying ρ, the maximum growth rate $\lambda_r = \gamma/2 - \alpha\kappa^2$ is obtained when the curly brackets on the right-hand side of Eq. (22) vanish, and this is possible for real ρ if

$$\frac{\delta}{2c'}\kappa^4 + \frac{\sigma^2 c^2}{c'^2}\kappa^2 \geqslant \frac{1}{4}; \tag{23}$$

moreover, condition (23) can be met if the perturbation wave number κ exceeds a certain lower cutoff value:

$$\kappa \geqslant \kappa_{\min} = \frac{\sigma c}{\sqrt{\delta c'}}\left\{\sqrt{1 + \frac{\delta c'^3}{2\sigma^4 c^4}} - 1\right\}^{1/2}. \tag{24}$$

Thus, the overall maximum of λ_r is realized for $\kappa = \kappa_{\min}$:

$$\lambda_r|_{\max} = \tfrac{1}{2}\gamma - \alpha\kappa_{\min}^2. \tag{25}$$

Out of all κ allowed by condition (24), the wave number $\kappa = \kappa_{\min}$ is selected here as it is the least affected by viscous dissipation. Furthermore, for $\kappa = \kappa_{\min}$, it follows from Eq. (22) that $\lambda_i = 0$, so according to Eqs. (20b) the most unstable perturbations have equal frequencies, $\omega_+ = \omega_- = \omega/2$.

According to Eq. (25), PSI arises if $\gamma > 2\alpha\kappa_{\min}^2$. The first term in the instability growth rate in Eq. (25) represents the destabilizing effect of resonant triad interactions while the second accounts for viscous dissipation, which is stabilizing. A similar result was obtained for the PSI of a sinusoidal plane wave in the absence of rotation [see Eq. (4.7) in Ref. [6]]; this is to be expected, as the vanishing group velocity of near-inertial subharmonic perturbations should not be a factor in the case of a periodic wave train where such perturbations are monochromatic [viz., Eqs. (19)].

In the inviscid limit ($\alpha = 0$), it follows from Eq. (25) that PSI is universal, and the maximum growth rate is $\gamma/2$ irrespective of the perturbation wavelength. This conclusion is in complete agreement with Young *et al.* [23]. More specifically, after converting to the present nondimensional variables, their expression (4.19) for the maximum PSI growth rate becomes $(3/8)\epsilon \sin\theta \cos\theta$; this is consistent with Eq. (25) in the inviscid limit ($\alpha = 0$), taking into account the slow time $T = \epsilon t$ and noting that, in view of Eqs. (4), (5), and (9), γ in Eq. (16) can be also expressed as $\gamma = (3/4)\sin\theta\cos\theta$.

IV. LOCALLY CONFINED BEAM

A. Eigenvalue problem

Next, we examine the stability of a beam with general locally confined profile $\overline{Q}(\eta)$ of $O(1)$ width (here the length scale L_* is chosen to be a measure of the beam width). For this purpose, we look for solutions of Eqs. (17) in the form of normal modes

$$A(\eta, T) = \hat{A}(\eta)e^{\lambda T}, \quad B(\eta, T) = \hat{B}(\eta)e^{\lambda^* T} \tag{26}$$

that decay far from the beam

$$\hat{A}, \hat{B} \to 0 \quad (\eta \to \pm\infty), \tag{27}$$

where $\lambda = \lambda_r + i\lambda_i$ is to be found. Upon inserting expressions (26) into Eqs. (17), $\hat{A}$ and $\hat{B}$ then satisfy

$$(\lambda + \alpha\kappa^2)\hat{A} + \frac{\sigma c}{\kappa}\hat{A}_\eta - \frac{i}{2}\frac{c'}{\kappa^2}\hat{A}_{\eta\eta} - i\delta\kappa^2|\overline{Q}_\eta|^2\hat{A} + \gamma\overline{Q}_{\eta\eta}\hat{B}^* = 0, \tag{28a}$$

$$(\lambda^* + \alpha\kappa^2)\hat{B} - \frac{\sigma c}{\kappa}\hat{B}_\eta - \frac{i}{2}\frac{c'}{\kappa^2}\hat{B}_{\eta\eta} - i\delta\kappa^2|\overline{Q}_\eta|^2\hat{B} + \gamma\overline{Q}_{\eta\eta}\hat{A}^* = 0. \tag{28b}$$

These equations along with the boundary conditions (27) define an eigenvalue problem with $\tilde{\lambda} = \lambda + \alpha\kappa^2$ as the eigenvalue parameter; thus, in terms of $\tilde{\lambda} = \tilde{\lambda}_r + i\tilde{\lambda}_i$, the instability criterion $\lambda_r > 0$ translates into $\tilde{\lambda}_r > \alpha\kappa^2$.

From the above eigenvalue problem it follows that PSI of a locally confined beam with profile $\overline{Q}(\eta)$ hinges on computing $\tilde{\lambda} = \tilde{\lambda}(f,\sigma,\kappa)$ and checking whether $\tilde{\lambda}_r > \alpha\kappa^2$. A comprehensive stability analysis thus involves varying three independent parameters: the background inertial frequency f, the detuning parameter σ which controls via Eq. (10) the proximity of the subharmonic frequency $\omega/2$ to f, and the perturbation wave number parameter κ. This rather formidable task becomes more manageable if $1 - f^2 \approx 1$, an approximation that is justified in ocean applications where $f \lesssim 0.1$. Under this assumption, f can be scaled out and, taking into account Eq. (16), Eqs. (28) simplify to

$$\hat{\lambda}\hat{A} + \sqrt{3}\frac{\hat{\sigma}}{\kappa}\hat{A}_\eta - i\frac{3}{2\kappa^2}\hat{A}_{\eta\eta} - i\frac{3\kappa^2}{2}|\overline{Q}_\eta|^2\hat{A} + \frac{3\sqrt{3}}{4}\overline{Q}_{\eta\eta}\hat{B}^* = 0, \tag{29a}$$

$$\hat{\lambda}^*\hat{B} - \sqrt{3}\frac{\hat{\sigma}}{\kappa}\hat{B}_\eta - i\frac{3}{2\kappa^2}\hat{B}_{\eta\eta} - i\frac{3\kappa^2}{2}|\overline{Q}_\eta|^2\hat{B} + \frac{3\sqrt{3}}{4}\overline{Q}_{\eta\eta}\hat{A}^* = 0, \tag{29b}$$

where

$$\hat{\lambda} = \frac{\lambda + \alpha\kappa^2}{f}, \quad \hat{\sigma} = \frac{\sigma}{f}. \tag{30}$$

Accordingly, the eigenvalue spectrum $\hat{\lambda} = \hat{\lambda}(\hat{\sigma},\kappa)$ now depends on two parameters, and in terms of $\hat{\lambda} = \hat{\lambda}_r + i\hat{\lambda}_i$ the instability criterion $\lambda_r > 0$ takes the form

$$\hat{\lambda}_r(\hat{\sigma},\kappa) > \mathbb{C}\kappa^2, \tag{31}$$

with

$$\mathbb{C} = \frac{\alpha}{f}. \tag{32}$$

It should be noted that Eqs. (29) admit a continuous spectrum of purely imaginary $\hat{\lambda}$, corresponding to radiating solutions far from the beam that are damped by viscosity. By contrast, solutions that are localized in the vicinity of the beam in keeping with the boundary conditions (27), and may give rise to instability, are associated with a discrete spectrum of isolated complex eigenvalues. The eigenvalue problem consisting of Eqs. (29) subject to conditions (27) has to be solved numerically in general.

The instability criterion (31) allows one to examine in a systematic way the PSI of a given beam profile $\overline{Q}(\eta)$, as follows: (i) solve Eqs. (29) subject to conditions (27) to compute the discrete eigenvalue spectrum, focusing entirely on modes with $\hat{\lambda}_r > 0$; (ii) plot $\hat{\lambda}_r$ as a function of wave number $\kappa > 0$, for various values of detuning $\hat{\sigma} \geqslant 0$; (iii) check whether these $\hat{\lambda}_r$ curves intersect with the quadratic $\mathbb{C}\kappa^2$ as we vary the parameter $\mathbb{C}$ defined in Eq. (32), which brings into the picture viscous dissipation [viz., Eq. (11)] and f. These intersections determine possible ranges of wave

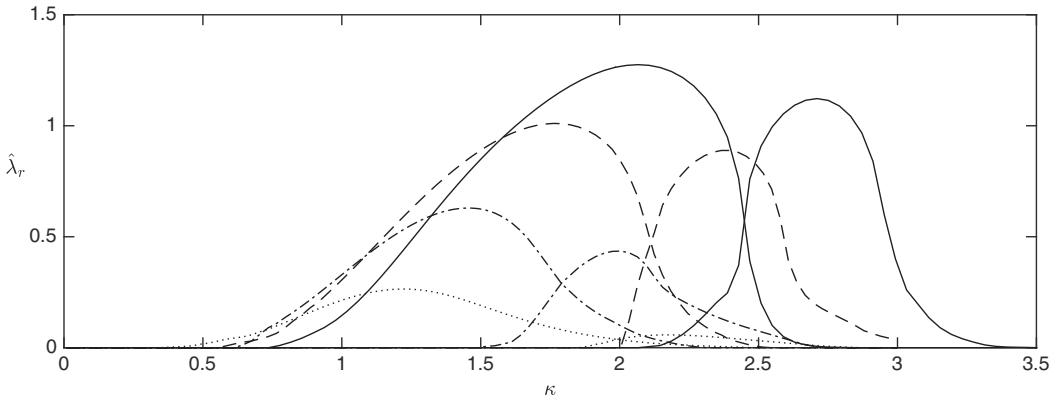

FIG. 2. Plots of the real part of stability eigenvalues $\hat{\lambda} = \hat{\lambda}_r + i\hat{\lambda}_i$ as function of the wave number parameter κ, for certain values of detuning $\hat{\sigma}$: solid line ($\hat{\sigma} = 0$); dashed line ($\hat{\sigma} = 2$); dashed-dotted line ($\hat{\sigma} = 3$); dotted line ($\hat{\sigma} = 4$). These eigenvalues were computed by solving Eqs. (29) subject to conditions (27) for the beam profile in Eq. (33).

numbers where the criterion (31) is satisfied; out of these unstable wave numbers, the most unstable perturbation corresponds to the wave number with the largest growth rate $\lambda_r = f\hat{\lambda}_r - \alpha\kappa^2$.

B. Gaussian beam profile

Here, we carry out the program outlined above using as an example the beam profile

$$\overline{Q}(\eta) = \frac{1}{\sqrt{8\pi}} \int_0^\infty e^{-l^2/8} e^{il\eta}\, dl. \tag{33}$$

This $\overline{Q}$ involves plane waves with wave numbers of the same sign ($l > 0$) and, as explained in Tabaei *et al.* [26], represents a unidirectional (progressive) beam that transports energy in the direction $x\cos\theta - y\sin\theta > 0$ along the beam. Furthermore, the beam stream function in Eq. (13a), at $t = 0$, is a Gaussian

$$\psi = \epsilon e^{-2\eta^2} \quad (t = 0), \tag{34}$$

with peak amplitude normalized to ϵ and standard deviation to $\frac{1}{2}$ (the characteristic length L_* is equal to twice the dimensional standard deviation). For the profile in Eq. (33), which satisfies $\overline{Q}(-\eta) = \overline{Q}^*(\eta)$, it is also straightforward to verify that if $\{\hat{\lambda}, \hat{A}(\eta), \hat{B}(\eta)\}$ is a solution to Eqs. (29) subject to the boundary conditions (27), so is $\{-\hat{\lambda}^*, -\hat{A}^*(-\eta), \hat{B}^*(-\eta)\}$; thus, discrete eigenvalues appear in pairs, and we select the mode with $\hat{\lambda}_r > 0$, as only it can be associated with instability.

Figure 2 shows plots of $\hat{\lambda}_r$ as a function of $\kappa > 0$ for $\hat{\sigma} = 0$, 2, 3, and 4. These numerical results were obtained by discretizing Eqs. (29) via second-order centered finite differences and applying the boundary conditions (27) at the edges of the computational domain, followed by generalized Schur decomposition of the resulting matrix eigenvalue problem. Specifically, we used the grid size $\Delta\eta = 0.01$ and the computational domain $-20 < \eta < 20$. As illustrated in Fig. 2, for each value of $\hat{\sigma}$, an eigenvalue branch first arises when κ exceeds a certain critical value, with two pairs of discrete eigenvalues $(\hat{\lambda}, -\hat{\lambda}^*)$ splitting off the continuous spectrum on the imaginary axis in the complex $\hat{\lambda}$ plane. [The numerical results strongly suggest that the two eigenvalue pairs, in fact, belong to the quartet $(\hat{\lambda}, -\hat{\lambda}, \hat{\lambda}^*, -\hat{\lambda}^*)$ so the unstable eigenvalues have the same $\hat{\lambda}_r$, but we have no rigorous proof for this claim.] Increasing κ beyond this bifurcation point, $\hat{\lambda}_r$ grows to a maximum and then drops off to zero at a finite κ, as the two eigenvalue pairs return to the imaginary axis. Before the first eigenvalue branch disappears, a new branch arises and follows a similar course to the previous one, and this pattern of successive bifurcations continues as κ is further increased; however, as argued

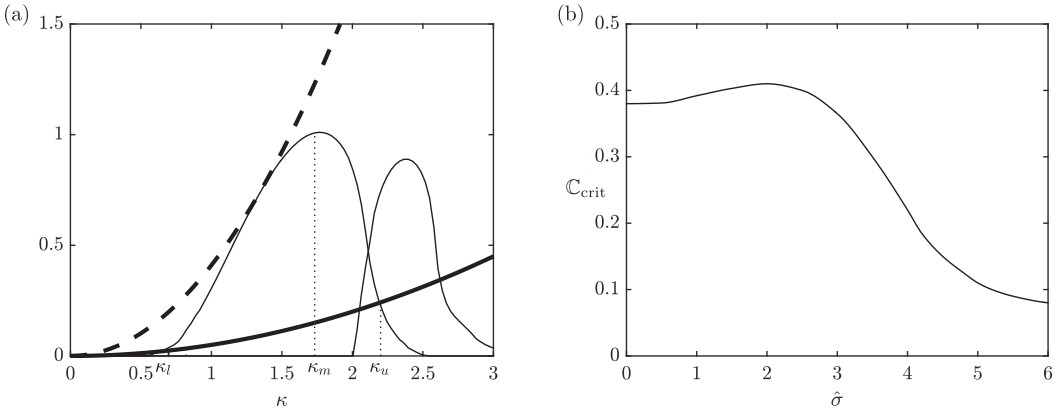

FIG. 3. Graphical implementation of the instability criterion (31) for detuning $\hat{\sigma} = 2$. (a) The quadratic $\mathbb{C}\kappa^2$ intersects with the primary eigenvalue branch $\hat{\lambda}_r(\kappa)$ in Fig. 2, and instability arises, only if $\mathbb{C} < \mathbb{C}_{\text{crit}} = 0.41$. The dashed parabola corresponds to the marginal situation $\mathbb{C} = \mathbb{C}_{\text{crit}}$ and the solid parabola to $\mathbb{C} = 0.05$, in which case there is a range of unstable wave numbers, $\kappa_l < \kappa < \kappa_u$, and the most unstable perturbation corresponds to $\kappa = \kappa_m$. (b) Dependence of $\mathbb{C}_{\text{crit}}$ on the detuning parameter $\hat{\sigma}$.

below, the primary branch plays the most important part in PSI analysis. We mention in passing that a countable infinity of eigenvalue branches was also found in the PSI analysis of quasimonochromatic beams with locally confined envelope and $f = 0$ [6].

Returning to the instability criterion (31), we now ask whether the quadratic $\mathbb{C}\kappa^2$ can intersect with the eigenvalue branches $\hat{\lambda}_r(\hat{\sigma},\kappa)$ computed above. The answer to this question hinges on $\hat{\sigma}$, which controls the tuning of near-inertial subharmonic perturbations [viz., Eqs. (10) and (30)], as well as the parameter $\mathbb{C} = \alpha/f$, where α measures viscous dissipation in comparison to nonlinear effects according to Eq. (11). As shown in Fig. 2, increasing $\hat{\sigma}$ causes the eigenvalue spectrum $\hat{\lambda}_r(\hat{\sigma},\kappa)$ to gradually shrink; thus, in the limit $\hat{\sigma} \gg 1$ and $\mathbb{C}$ fixed, no intersecting with $\mathbb{C}\kappa^2$ is expected. As a result, the beam profile in Eq. (33) may suffer PSI only if the subharmonic frequency $\omega/2$ is close enough to the inertial frequency f. This is consistent with the lack of PSI in the absence of background rotation, as concluded in Ref. [6] for beams with general locally confined profile.

The effect of varying the parameter $\mathbb{C}$ on PSI is illustrated in Fig. 3(a) for $\hat{\sigma} = 2$. It is seen that the quadratic $\mathbb{C}\kappa^2$ intersects with the primary eigenvalue branch, and hence PSI arises according to the criterion (31), only if $\mathbb{C} < \mathbb{C}_{\text{crit}} = 0.41$. When this condition is met, there are a range of unstable wave numbers $\kappa_l < \kappa < \kappa_u$, and the most unstable perturbation corresponds to $\kappa = \kappa_m$ for which the growth rate $\lambda_r = f(\hat{\lambda}_r - \mathbb{C}\kappa^2)$ is maximum. It should be noted that for $\mathbb{C} < 0.17$ the quadratic $\mathbb{C}\kappa^2$ also intersects with the second eigenvalue branch so there is an additional instability window. However, the threshold for PSI is set by $\mathbb{C}_{\text{crit}}$, and the most unstable perturbation is determined by the intersection of $\mathbb{C}\kappa^2$ with the primary eigenvalue branch. These findings are valid in general for $\hat{\sigma} \geqslant 0$, so the primary eigenvalue branch is always responsible for the dominant instability.

The dependence of $\mathbb{C}_{\text{crit}}$ on $\hat{\sigma}$ is displayed in Fig. 3(b). Interestingly, the maximum of $\mathbb{C}_{\text{crit}}$ occurs for $\hat{\sigma}$ positive ($\hat{\sigma} \approx 2$); thus, as $\mathbb{C} = \alpha/f$ is varied, PSI sets in when $\omega/2$ is slightly above f. This is illustrated in Fig. 4 which shows neutral curves $\alpha/f = \mathbb{C}_{\text{crit}}(\sigma/f)$ in the (f,σ) plane for three specific values of α. Each of these curves defines a stability boundary, to the right of which $\mathbb{C} < \mathbb{C}_{\text{crit}}$ and hence PSI is possible for the corresponding α. It should be noted that, for given α, f has to exceed a certain minimum $f = f_0$ for instability to be present; moreover, $\sigma > 0$ when $f = f_0$, confirming that the onset of PSI is realized for $\omega/2$ slightly above the inertial frequency. Beyond this threshold ($f > f_0$), PSI is possible for a finite range of σ, which translates into a window of near-inertial subharmonic frequencies according to Eq. (10). Furthermore, increasing α, thereby

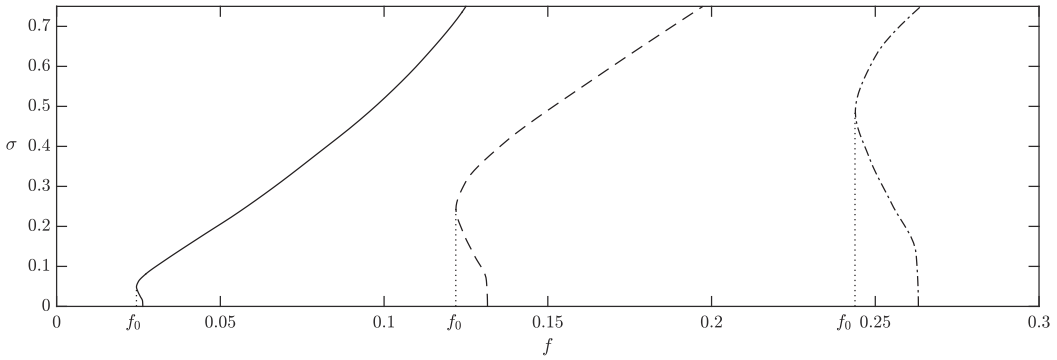

FIG. 4. Plots of neutral curves $\alpha/f = \mathbb{C}_{\text{crit}}(\hat{\sigma}/f)$ in the (f,σ) plane for three specific values of $\alpha = \nu/\epsilon^2$: solid line ($\alpha = 0.01$); dashed line ($\alpha = 0.05$); dashed-dotted line ($\alpha = 0.1$). To the right of each of these curves ($f > f_0$) PSI is possible for a finite range of σ.

amplifying viscous dissipation relative to nonlinear effects [viz., Eq. (11)], causes f_0 to increase as well.

By combining Eq. (32) with (11), the condition for PSI, $\mathbb{C} < \mathbb{C}_{\text{crit}}$, can also be expressed in terms of a threshold beam steepness:

$$\epsilon > \epsilon_{\text{crit}} = \sqrt{\frac{\nu}{f\mathbb{C}_{\text{crit}}(\hat{\sigma})}}. \tag{35}$$

This form of the instability condition underscores the competition of the destabilizing effect of resonant triad interactions, controlled by the beam steepness ϵ, against the viscous dissipation of the perturbations, measured by ν, and the tuning of near-inertial perturbations ($\omega/2 \approx f$), controlled by $\hat{\sigma}$ as discussed above.

C. Long-time evolution of PSI

The pump-wave approximation used in deriving the stability equations (17) eventually breaks down as unstable perturbations keep extracting energy from the underlying beam. The long-time development of the instability is governed by the nonlinear equation system (14) and (15) which accounts for the effect of the growing perturbations on the beam evolution.

To explore the entire instability process, from the early exponential growth of linear perturbations to the mature stage where subharmonic disturbances have reached comparable magnitude to the beam, Eqs. (14) and (15) were numerically solved using as initial condition the beam profile $\overline{Q}$ in Eq. (33), slightly perturbed by subharmonic disturbances in the form

$$Q(\eta,T=0) = \overline{Q}(\eta), \quad A(\eta,T=0) = B(\eta,T=0) = \frac{\overline{Q}(\eta)}{200}. \tag{36}$$

The numerical discretization employed second-order centered finite differences on a uniform grid with $\Delta\eta = 0.03$ in the computational domain $-100 < \eta < 100$, along with fourth-order Runge-Kutta time stepping with $\Delta T = 0.05$. The numerical results presented below were obtained taking $\mathbb{C} = 0.05$ and $\hat{\sigma} = 2$. For this choice of parameters, it follows from the eigenvalue analysis of Sec. IV B that linear instability arises for $0.63 < \kappa < 2.2$, as shown in Fig. 3(a); we chose $\kappa = 1.73$, which corresponds to the most unstable perturbation wave number $\kappa = \kappa_m$ in this range. Furthermore, we took $f = 0.1$, so $\sigma = 0.2$ and $\alpha = 5 \times 10^{-3}$ according to Eqs. (30) and (32).

Figure 5 summarizes the coupled evolution of the subharmonic disturbances and the underlying beam, for the initial conditions (36). The initial subharmonic perturbations quickly transform to a linear combination of the two unstable linear modes with eigenvalues $\hat{\lambda}$ and $\hat{\lambda}^*$, predicted by the

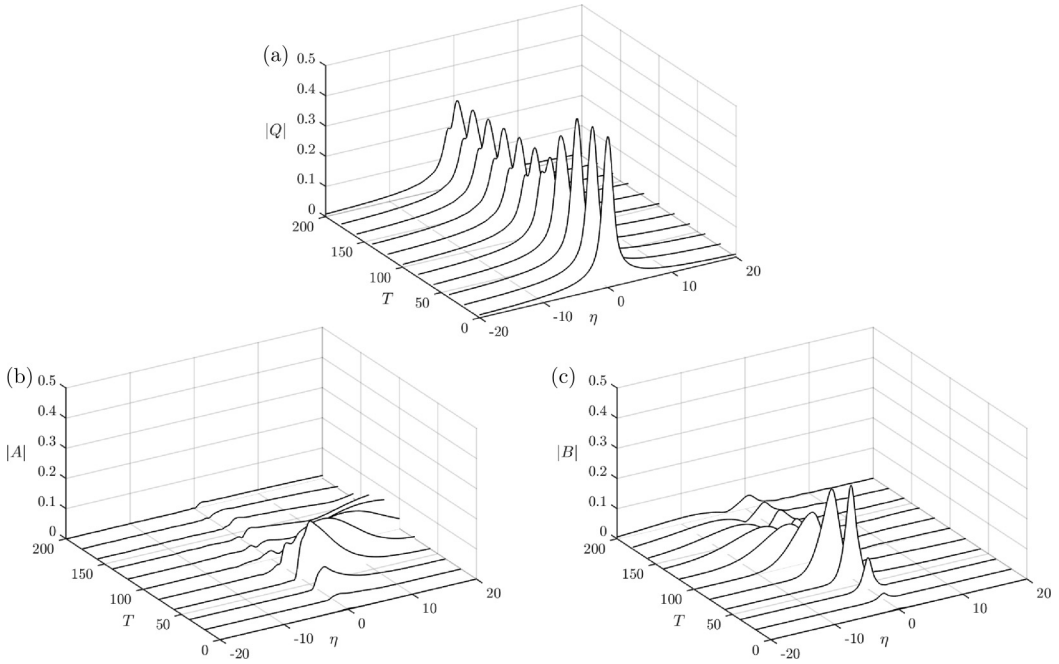

FIG. 5. Evolution of wave beam, with initially Gaussian stream function defined in Eq. (34), and subharmonic perturbations with the most unstable wave number according to linear stability analysis, for $f = 0.1$, $\hat{\sigma} = 2$, and $\mathbb{C} = 0.05$. The magnitudes of the beam profile ($|Q|$) and the perturbation envelopes ($|A|, |B|$) are displayed at various times T.

stability analysis of Sec. IV B, and this disturbance then grows exponentially with the appropriate linear growth rate $f\hat{\lambda}_r - \alpha\kappa_m^2$, while the beam remains essentially intact in line with the pump-wave approximation. The solution of the stability eigenvalue problem [viz., Eqs. (29) with the boundary conditions (27)] suggests that the (complex) eigenfunctions $(\hat{A}, \hat{B})$ of the two unstable modes obey the symmetries $|\hat{A}(\eta;\hat{\lambda})| = |\hat{B}(\eta;\hat{\lambda}^*)|$, $|\hat{A}(\eta;\hat{\lambda}^*)| = |\hat{B}(\eta;\hat{\lambda})|$. However, the mode with eigenvalue $\hat{\lambda}^*$, whose eigenfunction oscillates less rapidly than that of the mode with eigenvalue $\hat{\lambda}$ and matches the scale of $\overline{Q}(\eta)$ better, dominates the unstable disturbance that emerges from the assumed initial conditions (36); this explains the asymmetric evolution of $|A|, |B|$ in Fig. 5. The linear evolution stage lasts until $T \approx 40$. Beyond this time, as the perturbations have grown appreciably, the effect of the energy extracted from the beam becomes evident, with the beam peak amplitude dropping sharply between $T = 50$ and 80. As a result, for $T \gtrsim 80$, the subharmonic disturbances can no longer stay locked onto the beam. This signals the end of the nonlinear interaction, as the perturbations propagate away from the beam and eventually decay by viscous dissipation, leaving behind a beam with peak amplitude about half of the original. This depleted beam is confirmed to be stable based on the eigenvalue stability analysis of Sec. IV A.

V. DISCUSSION

We presented an asymptotic theory for PSI of an internal wave beam of frequency ω in the presence of background rotation, for the case where subharmonic perturbations have near-inertial frequency ($\omega/2 \approx f$). When this condition is met, beams of finite width are expected on physical grounds to be especially vulnerable to PSI, as near-inertial subharmonic perturbations have small group velocity and stay in contact with the underlying beam longer, thus extracting more energy, than subharmonic perturbations of general frequency. As expected for PSI, this energy transfer involves

perturbations that form resonant triads with the beam. Our analysis has shown that here resonant triad interactions are more robust than usual because of the small group velocity of near-inertial perturbations, and this fundamental difference of near-inertial PSI has important implications for beams of finite width.

Specifically, returning to expansions (13), the resonant triad conditions appropriate to near-inertial PSI can be expressed as

$$\boldsymbol{k}_+ + \boldsymbol{k}_- = O(1), \quad \omega_+ + \omega_- = \omega + O(\epsilon), \tag{37}$$

where $\boldsymbol{k}_\pm$ are the wave vectors and $\omega_\pm$ the frequencies of perturbations forming a triad with the underlying beam of $O(1)$ width and carrier frequency ω. These conditions were met in Eqs. (13) by our choice of carrier wave vectors $\pm\kappa/\epsilon^{1/2}\hat{\boldsymbol{e}}_\zeta$ and frequency $\omega/2$, in conjunction with $\eta = O(1)$ and $T = \epsilon t$ being the appropriate envelope variables, for the perturbations. By contrast, the analogous resonant triad conditions for generic PSI (ω not close to $2f$) take the form [see Eqs.(3.2) and (3.3) in Ref. [6]]

$$\boldsymbol{k}_+ + \boldsymbol{k}_- = \boldsymbol{k}_0 + O(\epsilon^{1/2}), \quad \omega_+ + \omega_- = \omega + O(\epsilon), \tag{38}$$

where $\boldsymbol{k}_0 = \hat{\boldsymbol{e}}_\eta$ is the carrier wave vector of the underlying beam, which in this instance is restricted to having nearly monochromatic profile with envelope of $O(1/\epsilon^{1/2})$ width. Furthermore, subharmonic perturbations that partake in resonant triads with such a beam, in keeping with Eqs. (38), have carrier wave vectors $\pm\kappa/\epsilon^{1/2}\hat{\boldsymbol{e}}_\zeta + \boldsymbol{k}_0/2$ and envelopes that depend on $\xi = \epsilon^{1/2}\eta$ and $T = \epsilon t$.

Upon comparison of Eqs. (37) with Eqs. (38), the frequency resonance condition is the same, and in both cases PSI involves fine-scale subharmonic wave packets of carrier frequency $\omega/2$ that evolve on an $O(1/\epsilon)$ time scale. The wave vector resonance condition, though, is far less binding for near-inertial than generic PSI. As a result, in the former case where Eqs. (37) apply, "thin" beams with locally confined profile of $O(1)$ width are susceptible to near-inertial PSI; whereas in the latter case, in accordance with Eqs. (38), PSI can arise only for relatively "wide" beams with nearly monochromatic profile of $O(1/\epsilon^{1/2})$ width. It should be noted that this crucial distinction between near-inertial and generic PSI is blurred if, instead of a finite-width beam, one considers an infinite sinusoidal wave train. Then, as discussed in Sec. III, the resonance conditions (37) are replaced by Eqs. (21), which are more akin to Eqs. (38), and the near-inertial PSI growth rate in Eq. (25) is similar to that found in Ref. [6] for PSI of a sinusoidal plane wave in the case $f = 0$.

The key role of near-inertial subharmonic perturbations in PSI of finite-width beams is supported by the numerical simulations of Gerkema *et al.* [18]. Using the nonlinear nonhydrostatic MIT-GCM, they explored the effect of latitude on the evolution of semidiurnal ($M2$) internal tide beams generated over the continental shelf break. Consistent with field observations of tidal beams originating from continental shelves [15], the beams seen in the simulations feature narrow profile (typical width-to-length ratio of 10^{-2}) with no distinct carrier; thus, based on the theory developed here, such beams would experience PSI to near-inertial subharmonic perturbations only. Indeed, out of the three latitudes examined in Gerkema *et al.* [18], strong instability is found only at 27.5°N, slightly below the critical latitude 28.8°N where the subharmonic $M2/2$ matches the local inertial frequency f. The salient features of this instability are consistent with those of near-inertial PSI discussed here: the dominant disturbances are at the $M1 = M2/2$ frequency and resemble short-scale wave packets with nearly horizontal crests; moreover, as a result of the instability, the beam loses a significant part of its energy so when it reaches the bottom it reflects as a linear wave. By contrast, no instability is found at 45°N and only traces of PSI are detected at the equator (0°N); in the latter instance, PSI drains very little of the beam energy, as evidenced by the generation of superharmonic reflected beams due to nonlinear effects [26], where the beam hits the ocean floor.

It is interesting to attempt a quantitative comparison of the instability found by Gerkema *et al.* [18] at 27.5°N with the predictions of our near-inertial PSI theory. To this end, we shall take the tidal beam to have Gaussian profile normalized as in Eq. (34), with $L_* = 500$ m so that the beam width ($\approx$4 standard deviations) is roughly 1 km, as estimated from Fig. 1 of Gerkema *et al.* [18]. According to the same figure, the peak beam velocity is about 0.15 m/s; combining this estimate with L_* and

the buoyancy frequency $N_0 = 2 \times 10^{-3}$ rad/s used in the simulations then gives $\epsilon = 0.12$ for the amplitude parameter in Eq. (34). Furthermore, the dimensionless semidiurnal frequency $\omega = 0.070$ and the dimensionless inertial frequency at 27.5°N $f = 0.034$ give $\sigma = 0.029$ according to Eqs. (5) and (9), so $\hat{\sigma} = \sigma/f = 0.85$. Finally, in regard to the parameter $\alpha = \nu/\epsilon^2$, Gerkema *et al.* [18] used different viscosity in the vertical and horizontal directions $\nu_* = 10^{-4}$ m^2/s and $\nu_* = 10^{-2}$ m^2/s, respectively; for both these values, the inverse Reynolds number defined in Eq. (2) turns out to be rather small, $\nu = 2 \times (10^{-7}, 10^{-5})$. Thus, viscous effects are relatively weak in comparison with nonlinear effects, as reflected in the corresponding $\alpha = 1.4 \times (10^{-5}, 10^{-3})$. As a result, the difference in viscosities does not affect significantly the most unstable perturbation wave number $\kappa = \kappa_m$ and corresponding maximum growth rate $\lambda_r|_{\max} = f\hat{\lambda}_r - \alpha\kappa_m^2$ obtained from solving the stability eigenvalue problem [viz., Eqs. (29) subject to conditions (27)] for the beam profile in Eq. (33) and $\hat{\sigma} = 0.85$. Specifically, for the two values of α above, we find $\kappa_m = (2.03, 2.00)$ and $\lambda_r|_{\max} = (0.042, 0.033)$. Taking into account the scaling of the perturbation wave number with $\epsilon^{-1/2}$ [viz., Eq. (8)] and restoring dimensions, the most unstable perturbation wavelength according to the theory is (536, 544) m, corresponding to approximately 2 wavelengths within the beam width. This overpredicts by a factor of about 2 the perturbation wavelength seen in Fig. 1 of Gerkema *et al.* [18]; however, in view of our crude assumptions about the beam profile and keeping in mind that $\epsilon^{1/2} = 0.34$ is not all that small, this rough agreement of the theory with the simulations seems reasonable. In regard to the instability growth rate, according to the simulations, the PSI kinetic energy grows by an order of magnitude in 2 days, which translates into an exponential growth rate of 1.15/days. On the other hand, the growth rate found theoretically [accounting for the scaling of the slow time in Eq. (12) and the fact that the kinetic energy grows at twice the rate of the stream function perturbation] turns out to be (1.72, 1.36)/days for the two values of α stated above. Again, this level of agreement of the asymptotic theory with the simulations is deemed satisfactory.

Finally, we wish to comment on the recent laboratory experiments by Maurer *et al.* [27] which examined the stability of finite-width beams for a range of background rotations f and beam frequencies ω. Similar to earlier laboratory experimental work for $f = 0$ by Bourget *et al.* [8], the beam profiles comprised roughly three wavelengths of a sinusoidal wave, and the observed instabilities are connected with perturbations that form resonant triads with the underlying beam. However, owing to the increased importance of viscous dissipation in the laboratory, the temporal and spatial scales of these triads do not adhere to those associated with PSI, and Maurer *et al.* [27] refer to the type of instability they observed as triadic resonant instability (TRI). Even though it is not feasible to make direct comparison of the present nearly inviscid ($\nu \ll 1$) theory for near-inertial PSI with the TRI observed in Ref. [27], our stability analysis provides a possible explanation for the unstable perturbations with subinertial frequency observed in these experiments for $\omega \approx 2f$. Unlike sinusoidal plane waves, which in keeping with the dispersion relation (4) cannot propagate with frequency below f, instability modes of a finite-width beam are evanescent far from the beam and the associated perturbations may have subinertial frequency. Specifically, according to Eqs. (13), (26), and (10), the perturbations corresponding to an instability eigenmode of a finite-width beam have frequencies

$$\omega_\pm = f + \left\{ \frac{\sigma^2(1 - f^2)}{2f} \mp \lambda_i \right\} \epsilon, \tag{39}$$

where $\lambda = \lambda_r + i\lambda_i$ is an unstable ($\lambda_r > 0$) eigenvalue obtained from Eqs. (28) subject to boundary conditions (27). This indicates that for σ sufficiently small (i.e., $\omega \to 2f$) one of the two unstable perturbations can have subinertial frequency.

ACKNOWLEDGMENT

This work was supported by the NSF under Grants No. DMS-1107335 and No. DMS-1512925.

APPENDIX: DERIVATION OF INTERACTION EQUATIONS

Here, we provide some intermediate steps in the derivation of the evolution equations (14) and (15). Upon substituting expansions (13) in the governing equations (1), interactions between the underlying beam and subharmonic perturbations arise due to the nonlinear terms in Eqs. (1). The contributions of each of these terms to the beam and perturbation harmonics, organized by phase, are

$$\begin{aligned} J(\rho,\psi) = {} & \frac{\epsilon^{5/2}}{\kappa}\left\{J\left(Fe^{i\kappa\zeta/\epsilon^{1/2}},Be^{-i\kappa\zeta/\epsilon^{1/2}}\right)+J\left(Ge^{-i\kappa\zeta/\epsilon^{1/2}},Ae^{i\kappa\zeta/\epsilon^{1/2}}\right)\right\}e^{-i\omega t} \\ & +\epsilon^2\left\{J\left(G^*e^{i\kappa\zeta/\epsilon^{1/2}},Q\right)+\frac{\epsilon^{1/2}}{\kappa}J\left(R,B^*e^{i\kappa\zeta/\epsilon^{1/2}}\right)\right\}e^{-i\omega t/2} \\ & +\epsilon^2\left\{J\left(F^*e^{-i\kappa\zeta/\epsilon^{1/2}},Q\right)+\frac{\epsilon^{1/2}}{\kappa}J\left(R,A^*e^{-i\kappa\zeta/\epsilon^{1/2}}\right)\right\}e^{-i\omega t/2}+\text{c.c.}, \end{aligned} \tag{A1}$$

$$\begin{aligned} J(w,\psi) = {} & \frac{\epsilon^{5/2}}{\kappa}\left\{J\left(Me^{i\kappa\zeta/\epsilon^{1/2}},Be^{-i\kappa\zeta/\epsilon^{1/2}}\right)+J\left(Ne^{-i\kappa\zeta/\epsilon^{1/2}},Ae^{i\kappa\zeta/\epsilon^{1/2}}\right)\right\}e^{-i\omega t} \\ & +\epsilon^2\left\{J\left(N^*e^{i\kappa\zeta/\epsilon^{1/2}},Q\right)+\frac{\epsilon^{1/2}}{\kappa}J\left(W,B^*e^{i\kappa\zeta/\epsilon^{1/2}}\right)\right\}e^{-i\omega t/2} \\ & +\epsilon^2\left\{J\left(M^*e^{-i\kappa\zeta/\epsilon^{1/2}},Q\right)+\frac{\epsilon^{1/2}}{\kappa}J\left(W,A^*e^{-i\kappa\zeta/\epsilon^{1/2}}\right)\right\}e^{-i\omega t/2}+\text{c.c.} \end{aligned} \tag{A2}$$

$$\begin{aligned} J(\nabla^2\psi,\psi) = {} & \frac{\epsilon^3}{\kappa^2}\left\{J\left(\mathbb{A}e^{i\kappa\zeta/\epsilon^{1/2}},Be^{-i\kappa\zeta/\epsilon^{1/2}}\right)+J\left(\mathbb{B}e^{-i\kappa\zeta/\epsilon^{1/2}},Ae^{i\kappa\zeta/\epsilon^{1/2}}\right)\right\}e^{-i\omega t} \\ & +\frac{\epsilon^{5/2}}{\kappa}\left\{J\left(Q_{\eta\eta},B^*e^{i\kappa\zeta/\epsilon^{1/2}}\right)+J\left(\mathbb{B}^*e^{i\kappa\zeta/\epsilon^{1/2}},Q\right)\right\}e^{-i\omega t/2} \\ & +\frac{\epsilon^{5/2}}{\kappa}\left\{J\left(Q_{\eta\eta},A^*e^{-i\kappa\zeta/\epsilon^{1/2}}\right)+J\left(\mathbb{A}^*e^{i\kappa\zeta/\epsilon^{1/2}},Q\right)\right\}e^{-i\omega t/2}+\text{c.c.}, \end{aligned} \tag{A3}$$

where

$$\mathbb{A}e^{i\kappa\zeta/\epsilon^{1/2}} \equiv \nabla^2 Ae^{i\kappa\zeta/\epsilon^{1/2}} = \left\{-\frac{\kappa^2}{\epsilon}A+2\frac{i\kappa}{\epsilon^{1/2}}\cos(\theta-\phi)A_\eta+A_{\eta\eta}\right\}e^{i\kappa\zeta/\epsilon^{1/2}}, \tag{A4}$$

$$\mathbb{B}e^{-i\kappa\zeta/\epsilon^{1/2}} \equiv \nabla^2 Be^{-i\kappa\zeta/\epsilon^{1/2}} = \left\{-\frac{\kappa^2}{\epsilon}B-2\frac{i\kappa}{\epsilon^{1/2}}\cos(\theta-\phi)B_\eta+B_{\eta\eta}\right\}e^{-i\kappa\zeta/\epsilon^{1/2}}. \tag{A5}$$

Combining Eq. (4) with (5) and invoking the near-inertial scaling $\sin\phi = \sigma\epsilon^{1/2}$, we also find

$$\sin\theta = s_0+\epsilon s_1+O(\epsilon^2), \tag{A6}$$

$$\cos\theta = c_0-\epsilon c_1+O(\epsilon^2), \tag{A7}$$

and

$$\cos(\theta-\phi) = c_0+\epsilon^{1/2}\sigma s_0-\epsilon\left(c_1+\frac{\sigma^2}{2}c_0\right)+O(\epsilon^{3/2}), \tag{A8}$$

where

$$s_0 = \sqrt{\frac{3f^2}{1-f^2}}, \quad s_1 = 2\sigma^2\sqrt{\frac{1-f^2}{3f^2}}, \quad c_0 = \sqrt{\frac{1-4f^2}{1-f^2}}, \quad c_1 = 2\sigma^2\sqrt{\frac{1-f^2}{1-4f^2}}. \tag{A9}$$

In addition, from Eq. (10), we have

$$\frac{1}{\omega} = w_0 - \epsilon w_1 + O(\epsilon^2), \tag{A10}$$

where

$$w_0 = \frac{1}{2f}, \quad w_1 = \sigma^2 \frac{1-f^2}{4f^3}. \tag{A11}$$

The evolution equation (14) for Q is derived by collecting terms proportional to $\exp(-i\omega t)$ in the governing equations (1), after substituting expansions (13). Making use of the first set of curly brackets in Eqs. (A1) and (A2), it follows from Eqs. (1a) and (1b), respectively,

$$R = -is_0 w_0 Q_\eta + \epsilon\left\{i(s_0 w_1 - s_1 w_0)Q_\eta - s_0 w_0^2 Q_{\eta T} + s_0 w_0 (AG - BF)_\eta\right\}, \tag{A12}$$

$$W = if c_0 w_0 Q_\eta + \epsilon\left\{-if(c_0 w_1 + w_1 c_0)Q_\eta + s_0 w_0 (AN - BM)_\eta + f c_0 w_0^2 Q_{\eta T}\right\}. \tag{A13}$$

Upon substituting Eqs. (A12) and (A13) into Eq. (1c) and using Eq. (A3), one then has

$$Q_T + s_0\left\{-\frac{s_0 w_0}{2}(AG - BF) + \frac{f c_0 w_0}{2}(AN - BM) + c_0 AB\right\} = 0. \tag{A14}$$

Next, we collect terms proportional to $\exp(\pm i\kappa\zeta/\epsilon^{1/2} - i\omega t/2)$. Specifically, making use of Eq. (A1), it follows from Eq. (1a) that

$$F = \epsilon^{1/2}\left\{2w_0\sigma A - \frac{2i w_0 s_0}{\kappa} A_\eta\right\} + \epsilon\left\{4\kappa w_0^2 s_0 \sigma Q_\eta B^* - 4i w_0^2 s_0^2 Q_\eta B_\eta^* - 2i w_0^2 s_0^2 Q_{\eta\eta} B^*\right\} + O(\epsilon^{3/2}), \tag{A15}$$

$$G = \epsilon^{1/2}\left\{-2w_0\sigma B - \frac{2i w_0 s_0}{\kappa} B_\eta\right\} + \epsilon\left\{4\kappa w_0^2 s_0 \sigma Q_\eta A^* + 4i w_0^2 s_0^2 Q_\eta A_\eta^* + 2i w_0^2 s_0^2 Q_{\eta\eta} A^*\right\} + O(\epsilon^{3/2}). \tag{A16}$$

Similarly, using Eq. (A2) in Eq. (1b) yields

$$\begin{aligned} M = {} & -2f w_0 A + \epsilon^{1/2}\left\{i\frac{2f w_0 c_0}{\kappa} A_\eta - 4f\kappa w_0^2 s_0 Q_\eta B^*\right\} + \epsilon\left\{-2i\alpha\kappa^2 w_0 M + 2f\left(\frac{w_0\sigma^2}{2} + w_1\right)A\right. \\ & + 4f\kappa w_0^2 c_0 \sigma Q_\eta B^* + 4if w_0^2 s_0 c_0 Q_\eta B_\eta^* + 8f\kappa^2 w_0^3 s_0^2 |Q_\eta|^2 A + 4if w_0^2 A_T \\ & \left. + 2if w_0^2 s_0 c_0 Q_{\eta\eta} B^*\right\} + O(\epsilon^{3/2}), \end{aligned} \tag{A17}$$

$$\begin{aligned} N = {} & 2f w_0 B + \epsilon^{1/2}\left\{i\frac{2f w_0 c_0}{\kappa} B_\eta - 4f\kappa w_0^2 s_0 Q_\eta A^*\right\} + \left\{-2i\alpha\kappa^2 w_0 N - 2f\left(\frac{w_0\sigma^2}{2} + w_1\right)B\right. \\ & + 4f\kappa w_0^2 c_0 \sigma Q_\eta A^* - 4if w_0^2 s_0 c_0 Q_\eta A_\eta^* - 8f\kappa^2 w_0^3 s_0^2 |Q_\eta|^2 B - 4if w_0^2 B_T \\ & \left. - 2if w_0^2 s_0 c_0 Q_{\eta\eta} A^*\right\} + O(\epsilon^{3/2}). \end{aligned} \tag{A18}$$

Inserting the leading order balance from the above,

$$F = O(\epsilon^{1/2}), \quad G = O(\epsilon^{1/2}), \quad M = -2f w_0 A, \quad N = 2f w_0 B, \tag{A19}$$

into Eq. (A14) produces

$$Q_T + s_0 c_0\left(2f^2 w_0^2 + 1\right)AB = 0. \tag{A20}$$

Substituting Eqs. (A9) and (A11) into (A20), we arrive at Eq. (14).

Finally, using Eq. (A3), it follows from Eq. (1c) that

$$A = -2fw_0M + \epsilon^{1/2}\left\{2w_0\sigma F + \frac{2ic_0}{\kappa}A_\eta - \frac{2iw_0s_0}{\kappa}F_\eta + \frac{2ifw_0c_0}{\kappa}M_\eta - 2\kappa w_0s_0Q_\eta B^*\right\}$$
$$+\epsilon\left\{\frac{2is_0\sigma}{\kappa}A_\eta + 2\kappa w_0c_0\sigma Q_\eta B^* + 2f\left(\frac{w_0\sigma^2}{2} + w_1\right)M + \frac{1}{\kappa^2}A_{\eta\eta} - 2iw_0A_T\right.$$
$$\left.+4iw_0s_0c_0Q_\eta B^*_\eta - 2i\alpha w_0\kappa^2 A\right\} + O(\epsilon^{3/2}), \tag{A21}$$

$$B = 2fw_0N + \epsilon^{1/2}\left\{-2w_0\sigma G - \frac{2ic_0}{\kappa}B_\eta - \frac{2iw_0s_0}{\kappa}G_\eta + \frac{2ifw_0c_0}{\kappa}N_\eta + 2\kappa w_0s_0Q_\eta A^*\right\}$$
$$+\epsilon\left\{-\frac{2is_0\sigma}{\kappa}B_\eta - 2\kappa w_0c_0\sigma Q_\eta A^* - 2f\left(\frac{w_0\sigma^2}{2} + w_1\right)N + \frac{1}{\kappa^2}B_{\eta\eta} - 2iw_0B_T\right.$$
$$\left.+4iw_0s_0c_0Q_\eta A^*_\eta - 2i\alpha w_0\kappa^2 B\right\} + O(\epsilon^{3/2}). \tag{A22}$$

Using Eqs. (A15) and (A17), we may then eliminate F and M from Eq. (A21) to obtain

$$-\left(4ifw_0^2 + 2iw_0\right)A_T + \frac{-8iw_0^2 + 2i}{\kappa}s_0\sigma A_\eta + \frac{1 - 4w_0^2\left(s_0^2 + f^2c_0^2\right)}{\kappa^2}A_{\eta\eta}$$
$$+\left[-4i\alpha\kappa^2 w_0 - 4f\left(\frac{w_0\sigma^2}{2} + w_1\right) + 4w_0^2\sigma^2\right]A\left(4 - 4fw_0 - 8f^2w_0^2\right)iw_0s_0c_0Q_\eta B^*_\eta$$
$$-8f\kappa^2w_0^3s_0^2|Q_\eta|^2A - (2 + 8fw_0)ifw_0^2s_0c_0Q_{\eta\eta}B^* = 0. \tag{A23}$$

Note that the $O(1)$ and $O(\epsilon^{1/2})$ terms in Eq. (A21) cancel out since $w_0 = (2f)^{-1}$ from Eq. (A11). Thus, after simplifying the coefficients in Eq. (A23) by making use of Eqs. (A9) and (A11), we arrive at Eq. (15a). Likewise, we use Eqs. (A16) and (A18) to eliminate G and N from Eq. (A22):

$$-\left(4ifw_0^2 + 2iw_0\right)B_T + \frac{8iw_0^2 - 2i}{\kappa}s_0\sigma B_\eta + \frac{1 - 4w_0^2\left(s_0^2 + f^2c_0^2\right)}{\kappa^2}B_{\eta\eta}$$
$$+\left[-4i\alpha\kappa^2 w_0 - 4f\left(\frac{w_0\sigma^2}{2} + w_1\right) + 4w_0^2\sigma^2\right]B$$
$$\times\left(4 - 4fw_0 - 8f^2w_0^2\right)iw_0s_0c_0Q_\eta A^*_\eta - 8f\kappa^2w_0^3s_0^2|Q_\eta|^2B$$
$$-(2 + 8fw_0)ifw_0^2s_0c_0Q_{\eta\eta}A^* = 0, \tag{A24}$$

and arrive at Eq. (15b) after using Eqs. (A9) and (A11) to simplify the coefficients in Eq. (A24).

[1] R. P. Mied, The occurrence of parametric instabilities in finite-amplitude internal gravity waves, J. Fluid Mech. **78**, 763 (1976).

[2] P. G. Drazin, On the instability of an internal gravity wave, Proc. R. Soc. Lond., Ser. A **356**, 411 (1977).

[3] C. R. Koudella and C. Staquet, Instability mechanisms of a two-dimensional progressive internal gravity wave, J. Fluid Mech. **548**, 165 (2006).

[4] C. Staquet and J. Sommeria, Internal gravity waves: from instabilities to turbulence, Annu. Rev. Fluid Mech. **34**, 559 (2002).

[5] B. R. Sutherland, The wave instability pathway to turbulence, J. Fluid Mech. **724**, 1 (2013).

[6] H. H. Karimi and T. R. Akylas, Parametric subharmonic instability of internal waves: Locally confined beams versus monochromatic wavetrains, J. Fluid Mech. **757**, 381 (2014).
[7] B. Bourget, H. Scolan, T. Dauxois, M. Le Bars, P. Odier, and S. Jouband, Finite-size effects in parametric subharmonic instability, J. Fluid Mech. **759**, 739 (2014).
[8] B. Bourget, T. Dauxois, S. Jouband, and P. Odier, Experimental study of parametric subharmonic instability for internal plane waves, J. Fluid Mech. **723**, 1 (2013).
[9] H. A. Clark and B. R. Sutherland, Generation, propagation, and breaking of an internal wave beam, Phys. Fluids **22**, 076601 (2010).
[10] A. Tabaei and T. R. Akylas, Nonlinear internal gravity wave beams, J. Fluid Mech. **482**, 141 (2003).
[11] D. E. Mowbray and B. S. Rarity, A theoretical and experimental investigation of the phase configuration of internal waves of small amplitude in a density stratified fluid, J. Fluid Mech. **28**, 1 (1967).
[12] L. Gostiaux, H. Didelle, S. Mercier, and T. Dauxois, A novel internal waves generator, Exp. Fluids **42**, 123 (2007).
[13] S. T. Cole, D. L. Rudnick, B. A. Hodges, and J. P. Martin, Observations of tidal internal wave beams at Kauai Channel, Hawaii, J. Phys. Oceanogr. **39**, 421 (2009).
[14] T. M. S. Johnston, D. L. Rudnick, G. S. Carter, R. E. Todd, and S. T. Cole, Internal tidal beams and mixing near Monterey Bay, J. Geophys. Res. **116**, C03017 (2011).
[15] R.-C. Lien and M. C. Gregg, Observations of turbulence in a tidal beam and across a coastal ridge, J. Geophys. Res. **106**, 4575 (2001).
[16] R. Fovell, D. Durran, and J. R. Holton, Numerical simulations of convectively generated stratospheric gravity waves, J. Atmos. Sci. **49**, 1427 (1992).
[17] H. H. Karimi, Parametric subharmonic instability of internal gravity wave beams, Ph.D. thesis, Department of Mechanical Engineering, MIT, 2015.
[18] T. Gerkema, C. Staquet, and P. Bouruet-Aubertot, Decay of semi-diurnal internal-tide beams due to subharmonic resonance, Geophys. Res. Lett. **33**, L08604 (2006).
[19] J. A. MacKinnon and K. B. Winters, Subtropical catastrophe: Significant loss of low-mode tidal energy at 28.9°, Geophys. Res. Lett. **32**, L15605 (2005).
[20] H. L. Simmons, Spectral modification and geographic redistribution of the semi-diurnal internal tide, Ocean Model. **21**, 126 (2008).
[21] J. A. MacKinnon, M. H. Alford, R. Pinkel, J. Klymak, and Z. Zhao, The latitudinal dependence of shear and mixing in the pacific transiting the critical latitude for PSI, J. Phys. Oceanogr. **43**, 3 (2013).
[22] G. S. Carter and M. C. Gregg, Persistent near-diurnal internal waves observed above a site of M2 barotropic-to-baroclinic conversion, J. Phys. Oceanogr. **36**, 1136 (2006).
[23] W. R. Young, Y.-K. Tsang, and N. J. Balmforth, Near-inertial parametric subharmonic instability, J. Fluid Mech. **607**, 25 (2008).
[24] A. D. McEwan, Interactions between internal gravity waves and their traumatic effect on a continuous stratification, Boundary–Layer Met. **5**, 159 (1973).
[25] M. J. Lighthill, *Waves in Fluids* (Cambridge University Press, Cambridge, 1978).
[26] A. Tabaei, T. R. Akylas, and K. G. Lamb, Nonlinear effects in reflecting and colliding internal wave beams, J. Fluid Mech. **526**, 217 (2005).
[27] P. Maurer, S. Joubaud, and P. Odier, Generation and stability of inertia–gravity waves, J. Fluid Mech. **808**, 539 (2016).